Time-Lapse Seismic Crosswell Monitoring of Steam Injection in Tar Sand

Jesper Spetzler, Dept. of Geotechnology, Delft University of Technology, The Netherlands.*

Summary

Time-lapse tomography of crosswell seismic data can be used to monitor hydrocarbon reservoirs for P-wave velocity changes due to production over time. A finite-frequency wave theory for phase and amplitude attributes is applied in the forward modelling part. In the inversion part, the common problem of poor illumination in crosswell tomography is taken into account. The developed tomographic imaging technique is used on real data in a crosswell experiment with two source wells and two receiver wells (i.e., in total there are four cross sections). Hot steam was injected via a horizontal pipeline going through a reservoir of tar sand during 72 days between the baseline and monitor survey. The time delay and relative amplitude variation observed in the time-lapse data were used separately and jointly to estimate the time-lapse velocity models for all four cross sections. In general, the four cross sections show a negative velocity anomaly close to the pipeline location. This observation is in agreement with rock physics modelling experiments that a temperature increase results in a velocity reduction of heavy oil reservoirs.

Introduction

Time-lapse seismic monitoring has gained increasing popularity in the last years as a tool to estimate the temporal changes in velocity and stress conditions of hydrocarbon reservoirs. In most cases, the 4D changes of reservoir parameters are determined from reflection data recorded over reservoirs at several kilometres depth. Such reflection seismic experiments have resulted in valuable insight into reservoir changes inherent to production, as well as, the productivity of the reservoirs is improved. In a similar vein to reflection experiments, it is possible to time-lapse monitor hydrocarbon reservoirs in transmission experiments such as crosswell tomography. With an improved tomographic technique taking the finite-frequency effect of wavefields into account, both phase and amplitude attributes from time-lapse seismic crosswell data can be used separately or jointly to compile velocity models of the temporal changes between two data sets. In addition, the developed tomographic imaging method corrects for the problem of poor illumination that is common in crosswell tomography. The improved tomographic approach is applied on real data from a crosswell experiment where steam is injected into a formation of tar sand.

Finite-Frequency Phase and Amplitude Attributes

The finite-frequency wave theory for phase and amplitude attributes is presented in this section. The Rytov wavefield $P_R(\mathbf{r}_r, \mathbf{r}_s, \omega)$ at the angular frequency emitted $\omega = 2\pi f$ (f is the frequency) from the source position $\mathbf{r}_s$ and recorded at the receiver position $\mathbf{r}_r$ is given by

$$P_R(\mathbf{r}_r, \mathbf{r}_s, \omega) = P_0(\mathbf{r}_r, \mathbf{r}_s, \omega) \exp\left(\frac{P_B}{P_0}(\mathbf{r}_r, \mathbf{r}_s, \omega)\right), \qquad (1)$$

The monochromatic reference wavefield is denoted by $P_0(\mathbf{r}_r, \mathbf{r}_s, \omega)$. The first order Born wavefield is given by $P_B(\mathbf{r}_r, \mathbf{r}_s, \omega)$ at angular frequency ω. The single-scattering process of a propagating wavefield in a heterogeneous medium is included in the exponential function of Eq. (1). This exponential function is a complex number. The angle and norm of the complex number return the travel time delay (i.e., phase delay divided by the angular frequency) and the relative amplitude variation, respectively. The relative amplitude variation is divided by the angular frequency so that both the phase and amplitude attribute will have be on the same order of magnitude. Hence, the traveltime shift and the frequency divided relative amplitude variation inherent to velocity perturbations are given by

$$\Delta t(\mathbf{r}_r, \mathbf{r}_s) = \int_{-\infty}^{\infty} \int_0^L \Delta v(z, r) K_{\Delta t}(z, r) dz dr, \qquad (2)$$

and

$$\frac{\Delta A}{A_0}(\mathbf{r}_r, \mathbf{r}_s) = \int_{-\infty}^{\infty} \int_0^L \Delta v(z, r) K_{\Delta A}(z, r) dz dr, \qquad (3)$$

respectively. The functional K with the subscripts Δt or ΔA is known as the Fréchet kernel or the sensitivity function for either the phase or amplitude attribute. The integration in Eqs. (2) and (3) is carried out over the volume between the source and receiver. For a homogeneous 2D reference velocity model the Fréchet kernel for the phase attribute equals

$$\begin{aligned} K_{\Delta t}^{2D}(x, z) &= -\sqrt{\frac{L}{v_0^5 x(L-x)}} \int_{f_0-\Delta f}^{f_0+\Delta f} \mathcal{A}(f) \\ &\quad \times \sqrt{f} \sin\left(\frac{f\pi L z^2}{v_0 x(L-x)} + \frac{\pi}{4}\right) df, \end{aligned} \qquad (4)$$

and the 2D sensitivity function for the amplitude attribute is given by

$$\begin{aligned} K_{\Delta A}^{2D}(x, z) &= -\sqrt{\frac{L}{v_0^5 x(L-x)}} \int_{f_0-\Delta f}^{f_0+\Delta f} \mathcal{A}(f) \\ &\quad \times \sqrt{f} \cos\left(\frac{f\pi L z^2}{v_0 x(L-x)} + \frac{\pi}{4}\right) df. \end{aligned} \qquad (5)$$

A coordinate system with origin at the source position, the x-axis aligned with the source-receiver line and the z-axis perpendicular to the source-receiver line is used to derive Eqs. (4) and (5). The distance between the source and receiver is denoted by L. Time delays and relative amplitude variations of seismic data are always estimated over a broad frequency band, thus the Fréchet kernels in Eqs. (4) and (5) include the frequency integration $[f_0 - \Delta f; f_0 + \Delta f]$ for which the normalised amplitude spectrum $\mathcal{A}(f)$ of the observed wavefield satisfies that $\int_{f_0-\Delta f}^{f_0+\Delta f} \mathcal{A}(f)df = 1$. See Woodward (1992) and Spetzler and Snieder (2004) for more information about the Rytov approximation and how obtain the travel time delay and fractional amplitude sensitivity kernels.

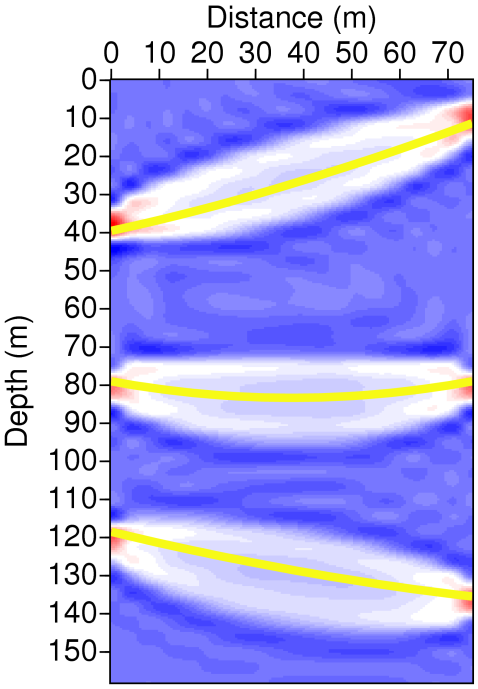

Fig. 1: Time delay sensitivity kernels and ray paths.

For wave propagation in 3D media, Eqs (2) and (3) are still valid but with other Fréchet kernels than in Eqs. (4) and (5). In addition, the finite-frequency wave theory for phase and amplitude attributes works well for heterogeneous reference media. In that case, ray bending effects are taking into account when computing the sensitivity functions (i.e., in the computation of traveltime and geometrical spreading factor). Fig. 1 shows an example of time delay Fréchet kernels and ray paths for three shot-receiver combinations in a crosswell experiment. The source well is to the left at 0 meter, and the receiver well is to the right at 75 meter. The ray paths are indicated with the yellow lines, while the finite-frequency sensitivity kernels are plotted with the red, blue and white colours. The white area is the part of the Fréchet kernels with highest sensitivity. This area corresponds to the first Fresnel zone. Notice that the sensitivity of the finite-frequency sensitivity kernels is non-zero away from the ray path and is continuous over the first Fresnel zone. In contrast, the ray theory only defines non-zero sensitivity to velocity perturbations along the ray path. The Fréchet kernels for the relative amplitude attribute are similar to the time shift sensitivity kernels in Fig. 1.

Properties of the Linear Wave Theory

In contrast to the well-known ray theory that is based a high-frequency approximation, the linear wave theory accounts for the finite-frequency (FF) features of propagating waves. It turns out that the linear wave theory is a natural extension of ray theory. One can show that in the high-frequency limit the time delay predicted in Eq. (2) equals the time shift computed with ray theory (RT), hence

$$\lim_{f\to\infty} \Delta t|_{\mathrm{FF}}(\mathbf{r}_r, \mathbf{r}_s) = \Delta t|_{\mathrm{RT}}(\mathbf{r}_r, \mathbf{r}_s), \tag{6}$$

In the high-frequency limit, the effect of single wave scattering on the amplitude vanishes. However, the impact of geometrical spreading factor as predicted by ray theory still remains. Hence, in the high-frequency limit the fractional amplitude in Eq. (3) converges to the ray theoretical result that

$$\lim_{f\to\infty} \frac{\Delta A}{A_0}|_{\mathrm{FF}}(\mathbf{r}_r, \mathbf{r}_s) = \frac{\Delta A}{A_0}|_{\mathrm{RT}}(\mathbf{r}_r, \mathbf{r}_s), \tag{7}$$

which includes the effect of geometrical spreading factor. The result in Eq. (6) and (7) holds for wave propagation in 3D as well.

Regime of the Linear Wave Theory

The finite-frequency wave theory is important for heterogeneous media with structures smaller in size a than the Fresnel volume $L_F = \sqrt{\lambda L}$, where the wavelength is denoted by λ. Hence,

$$L_F/a > 1. \tag{8}$$

On the contrary, the regime of ray theory is that

$$\lambda/a < 1 \qquad \text{and} \qquad L_F/a < 1. \tag{9}$$

Time-Lapse Monitoring of Steam Injection in Tar Sand

The time-lapse crosswell experiment is located in the Alberta province of Canada. In between the baseline and monitor survey, steam was injected in a formation of tar sand (i.e., heavy oil) through a horizontal pipeline between the source and receiver wells. The steam injection lasted 72 between the baseline and monitor survey. Thereby, the reservoir of heavy oil was heated up by conduction in order to make the bitumen less viscous. Paulsson *et al.* (1994) provide more details about the 4D steam injection experiment.

The crosswell experiment is configured with two source wells (i.e., CH1 and CH4) and two receiver wells (i.e., CH2 and CH3). A sketch of the acquisition geometry is presented in Fig. 2. The horizontal pipeline at 250 m depth with steam injection is indicated with the red arrows. In total, there are four cross sections, hence making it possible to estimate a pseudo 3D time-lapse velocity model. The sources and receivers are located between 160 m and 320 meters depth with a vertical increment of 2 meter for both sources and receivers. The source energy is generated by a prototype P-wave and S-wave source vibrator that has been invented by Paulsson Geophysical Services. The source position is well-repeated in the monitor survey, which contributes to only minor non-repeatability effects in the time-lapse data set. In addition, the source signature is very repeatable because of the use a mechanical tool. The two 80 level receiver arrays are permanently cemented in the well casing, hence the coupling is good and the repeatability of receiver positioning in the time-lapse data set is perfect. In general, the time-lapse data set is of a very high quality and there are few problems with non-repeatability effects due to differences in acquisition.

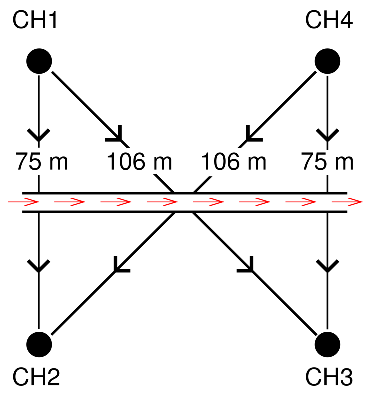

Fig. 2: Acquisition geometry of the pseudo 3D crosswell experiment.

Data Processing

After removal of zero traces in the data set, more than 5500 traces with waveform data are available for the tomographic inversion. The first arrivals are very clear in the data. A Fourier analysis shows that the strongest energy part is between 200 Hz and 600 Hz. The ray path coverage for the cross section CH4CH3 is shown in Fig. 3. Most ray paths go through the centre of the target area while the top and bottom part are poorly sampled areas. Notice the undersampled area at 260 meter depth that is a result of zero energy shotgathers. The figure shows an example of the general problem of poor illumination in crosswell tomography. The black cross indicates the position of the horizontal steam pipeline. 2D Fréchet kernels are used in the experiment though the recorded seismic wavefields propagate in 3D. The 3D reference model is 2.5D. In that case, one can show by using the stationary phase approximation that the 3D Fréchet kernels converge to the 2D Fréchet kernels.

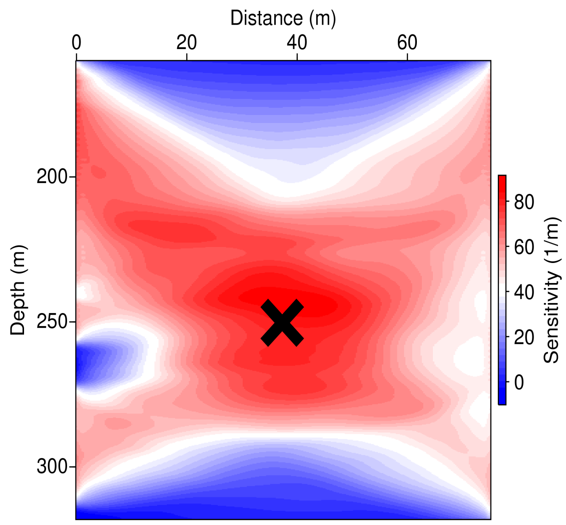

Fig. 3: Ray path coverage for cross section CH4CH3.

Processing scheme for the crosswell seismic data:

1. A reference model was defined for computation of the sensitivity kernels and reference traveltimes.
2. A time window around the first arrival using the reference travel times was defined.
3. The time-windowed first arriving energy was filtered between 200 Hz and 600 Hz.
4. A spectral ratio method was applied on the time-lapse data to obtain the travel time delays and the relative amplitude variation estimates for all traces in the time-lapse data set.

The time delay and relative amplitude attributes from the time-lapse data were used to estimate 4D velocity structure and strength inherent to steam injection between the baseline and monitor survey. I used a linear inversion method that can take non-uniform ray path coverage into account. In this approach, 2D Fourier functions are used to express the time-lapse velocity field $\Delta v(\mathbf{r})$ at coordinate position $\mathbf{r}$. Hence, the time-lapse velocity field is given by

$$\Delta v(\mathbf{r}) = \sum_{i=1}^{\infty}\sum_{j=1}^{\infty} c_{ij} B_i(\mathbf{r}) B_j(\mathbf{r}). \qquad (10)$$

In practice the summation is limited to a finite integer number. The unknown coefficients c_{ij} are estimated by inversion. Afterwards, the time-lapse velocity field is computed from Eq. (10). In the case that the non-uniform ray path coverage is not accounted for, estimated models in crosswell tomographic experiments can be significantly biased.

A standard linear least squares inversion is applied to compute the estimated model vector $\tilde{m}$ with the coefficients c_{ij} from the time shift and relative amplitude variation attributes. Hence,

$$\tilde{m} = [\mathbf{A}^t \mathbf{C}_D^{-1} \mathbf{A} + \mathbf{C}_M^{-1}]^{-1} \mathbf{A}^t \mathbf{C}_D^{-1} d. \quad (11)$$

The modelling matrix is given by $\mathbf{A}$, the data and model covariance matrix are denoted $\mathbf{C}_D$ and $\mathbf{C}_M$, respectively, while the data vector with the time delays and/or the amplitude ratio attributes is written as d. It is necessary to use a regularisation condition to stabilise the inversion problem. The value of the regularisation parameter is carefully chosen as small as possible in order to minimise the effect on the strength of the velocity anomaly.

Time-Lapse Tomographic Results

The estimated time-lapse velocity models using the traveltime delay and the relative amplitude variation for cross section CH4CH3 are illustrated in Fig. 4, respectively. By inspection, it is seen that the inverted models are similar in the sense that they show a negative velocity anomaly in the area around the horizontal pipeline. This is an encouraging result because it is generally known from rock physics modelling that in heavy oil sandstone reservoirs a temperature increment is correlated with a velocity reduction, see Paulsson *et al.* (1994) and Mavko *et al.* (2003). I have compiled the tomographic images for the three remaining cross sections using the delay time and relative amplitude attributes separately and jointly in the inversion. All the cross sections show the presence of a negative velocity anomaly near the pipeline location. (Only the two cross sections in Fig. 4 of a total of 3×4 cross sections for time delay and amplitude attributes are presented in the paper to due the lack of space.)

Conclusions

I used tomography to image the pseudo 3D time-lapse structure of a heavy oil reservoir in which steam had been injected. I applied a finite-frequency wave theory for phase and relative amplitude variation attributes. These two seismic attributes were estimated from the direct P-wave arrivals in a time-lapse data set by using a spectral ratio approach. The inversion approach included a correction for the bias due to poor illumination that is a general problem is crosswell tomography. The inverted time-lapse velocity models for all four cross sections show a significant negative velocity anomaly in the vicinity of the horizontal pipeline. This observation is in agreement with rock physics modelling that a temperature increase will decrease the P-wave velocity in a tar sand reservoir.

Acknowledgements

This work is sponsored by the Dutch technology organisation STW through the project no. DAR.6293. Paulsson Geophysical Services is acknowledged for making the crosswell data set available to this study.

References

Mavko, G., Mukerji, T., and Dvorkin, J., 2003, The rock physics handbook: Cambridge university press.

Paulsson, B., Meredith, J., Wang, Z., and Fairborn, J., 1994, The steepbank crosswell seismic project: Reservoir definition and evaulation of steamflood technology in alberta tar sands: The Leading Edge, pages 737–747.

Spetzler, J., and Snieder, R., 2004, Tutorial: The fresnel volume and transmitted waves: Geophysics, **69**, 653–663.

Woodward, M. J., 1992, Wave-equation tomography: Geophysics, **57**, 15–26.

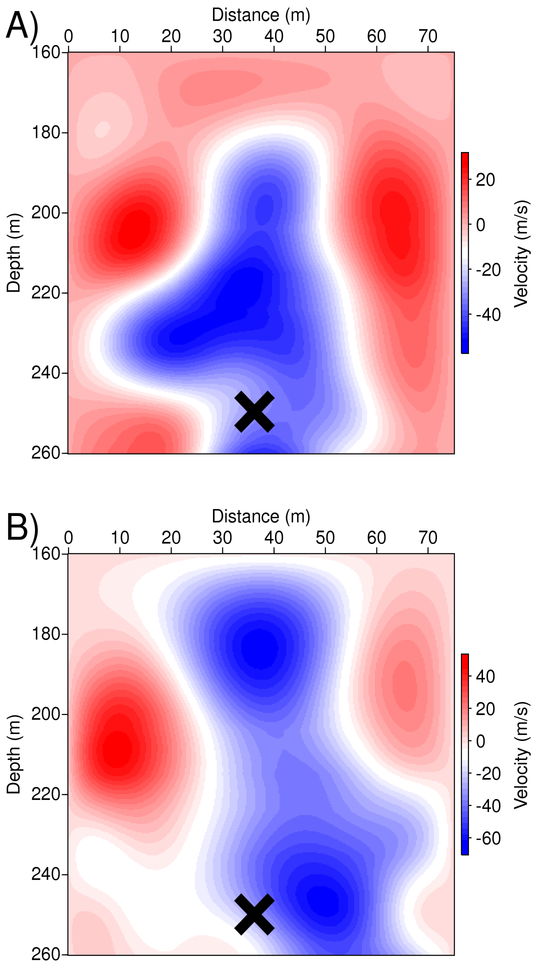

Fig. 4: Estimated time-lapse velocity structure for cross section CH4CH3. (A) Inversion of phase attribute. (B) Inversion of amplitude attribute. The cross indicates the location of the horizontal stream pipeline.

EDITED REFERENCES

Note: This reference list is a copy-edited version of the reference list submitted by the author. Reference lists for the 2006 SEG Technical Program Expanded Abstracts have been copy edited so that references provided with the online metadata for each paper will achieve a high degree of linking to cited sources that appear on the Web.

REFERENCES

Mavko, G., T. Mukerji, and J. Dvorkin, 2003, The rock physics handbook: Cambridge University Press.

Paulsson, B., J. Meredith, Z. Wang, and J. Fairborn, 1994, The steepbank crosswell seismic project: Reservoir definition and evaulation of steamflood technology in alberta tar sands: The Leading Edge, **13**, 737–747.

Spetzler, J., and R. Snieder, 2004, Tutorial: The fresnel volume and transmitted waves: Geophysics, **69**, 653–663.

Woodward, M. J., 1992, Wave-equation tomography: Geophysics, **57**, 15–26.